Experimental calibration and validation of sewer/surface flow exchange equations in steady and unsteady flow conditions

Rubinato, M, Martins, R, Kesserwani, G, Leandro, J, Djordjević, S & Shucksmith, J

DOI 10.1016/j.jhydrol.2017.06.024
ISSN 0022-1694
ESSN 1879-2707

Publisher: Elsevier

Journal of Hydrology 552 (2017) 421–432

Contents lists available at ScienceDirect

Journal of Hydrology

journal homepage: www.elsevier.com/locate/jhydrol

Research papers

Experimental calibration and validation of sewer/surface flow exchange equations in steady and unsteady flow conditions

Matteo Rubinato [a,*], Ricardo Martins [a,b,c], Georges Kesserwani [a], Jorge Leandro [d,b,c], Slobodan Djordjević [e], James Shucksmith [a]

[a] Dept. of Civil and Structural Engineering, Mappin Building, S1 3JD University of Sheffield, Sheffield, UK
[b] MARE – Marine and Environmental Sciences Centre, Department of Civil Engineering, Faculty of Sciences and Technology, University of Coimbra, 3004-517 Coimbra, Portugal
[c] IMAR – Institute of Marine Research, Faculty of Sciences and Technology, University of Coimbra, 3004-517 Coimbra, Portugal
[d] Department of Civil, Geo and Environmental Engineering, Chair of Hydrology and River Basin Management, Technical University of Munich, Arcisstrasse 21, 80333 Munich, Germany
[e] Centre for Water Systems, University of Exeter, North Park Road, Exeter EX4 4QF, UK

ARTICLE INFO

Article history:
Received 27 October 2016
Received in revised form 14 June 2017
Accepted 15 June 2017
Available online 17 June 2017
This manuscript was handled by Corrado Corradini, Editor-in-Chief, with the assistance of Gokmen Tayfur, Associate Editor

Keywords:
Sewer and free surface interactions
Discharge coefficients
Experimental and numerical validations
Steady and unsteady modelling

ABSTRACT

The linkage between sewer pipe flow and floodplain flow is recognised to induce an important source of uncertainty within two-dimensional (2D) urban flood models. This uncertainty is often attributed to the use of empirical hydraulic formulae (the one-dimensional (1D) weir and orifice steady flow equations) to achieve data-connectivity at the linking interface, which require the determination of discharge coefficients. Because of the paucity of high resolution localised data for this type of flows, the current understanding and quantification of a suitable range for those discharge coefficients is somewhat lacking. To fulfil this gap, this work presents the results acquired from an instrumented physical model designed to study the interaction between a pipe network flow and a floodplain flow. The full range of sewer-to-surface and surface-to-sewer flow conditions at the exchange zone are experimentally analysed in both steady and unsteady flow regimes. Steady state measured discharges are first analysed considering the relationship between the energy heads from the sewer flow and the floodplain flow; these results show that existing weir and orifice formulae are valid for describing the flow exchange for the present physical model, and yield new calibrated discharge coefficients for each of the flow conditions. The measured exchange discharges are also integrated (as a source term) within a 2D numerical flood model (a finite volume solver to the 2D Shallow Water Equations (SWE)), which is shown to reproduce the observed coefficients. This calibrated numerical model is then used to simulate a series of unsteady flow tests reproduced within the experimental facility. Results show that the numerical model overestimated the values of mean surcharge flow rate. This suggests the occurrence of additional head losses in unsteady conditions which are not currently accounted for within flood models calibrated in steady flow conditions.

1. Introduction

The increased frequency and magnitude of worldwide flood events in recent years (Ravazzani et al., 2016) has encouraged a critical examination of possible causes (Hundecha et al., 2016) and suitable options to reduce their impact. Urban flooding may occur when storm water exceeds the capacity of the local sewer or storm water system. Dual drainage hydraulic models have been developed to assess the risks associated with urban flooding, namely the potential damage to property and infrastructure (Martins et al., 2016; Mark et al., 2004), and to supply information for decision makers (Fernandez et al., 2016). Such modelling tools use steady state linking discharge equations to enable the coupling of below-ground pipe flow and free surface flow at computational (interface) nodes representing manholes/gullies (e.g. Leandro et al., 2009; Lee et al., 2015; Maksimović et al., 2009). In such forms of integrated flood modelling, interaction discharges are usually added as sinks or sources within the overland flow model (e.g. Seyoum et al., 2012; Chen et al., 2015; Leandro and Martins, 2016; Martins et al., 2016).

* Corresponding author.
E-mail addresses: m.rubinato@sheffield.ac.uk (M. Rubinato), Ricardo.Martins@sheffield.ac.uk (R. Martins), g.kesserwani@shef.ac.uk (G. Kesserwani), jorge.leandro@tum.de (J. Leandro), S.Djordjevic@exeter.ac.uk (S. Djordjević), j.shucksmith@sheffield.ac.uk (J. Shucksmith).

http://dx.doi.org/10.1016/j.jhydrol.2017.06.024
0022-1694/

State-of-the-art dual drainage models (Smith, 2006) couple 1D (one-dimensional) sewer network flow models to 2D floodplain model (Chen et al., 2015; Leandro et al., 2009; Lee et al., 2013; Schmitt et al., 2004) utilising weir or orifice equations to describe flow exchange between the surface and sewer systems as a function of relative hydraulic head in the sewer and surface systems (Djordjević et al., 2005; Chen et al., 2007). These discharge relationships were derived using the principles of energy or momentum conservation assuming a steady state flow, with discharge coefficient comprising energy losses. Nonetheless they are commonly employed within unsteady flow simulators on the assumption that the computational time step is small (i.e. dV/dt is assumed constant at each time step, V is the volume of flow). In reality, flows through these interaction nodes during flood events are highly complex, transient and three dimensional, with surcharge/drainage affecting local hydrodynamics around the interaction node, and the flow direction potentially altering several times during a flooding event (Balmforth et al., 2006). Although it may be more appropriate to apply 3D models to replicate such systems, equivalent models are computationally demanding and hence not applicable to real urban inundation events (Cea et al., 2010). In these cases the use full shallow water equation models or simplified models neglecting the inertial terms is deemed acceptable (Mignot et al., 2006). The representation of surface/subsurface flow exchange and energy loss processes is recognised as a potential source of uncertainty within urban flood models (Djordjević et al., 2005), especially because little guidance exists on a range of suitable weir/orifice discharge coefficients for use in a flood modelling context.

The three dimensional and rapidly changing nature of interaction flows mean that the accurate characterisation of hydraulic conditions around interaction nodes is extremely challenging. The uncertain nature of flood events and the difficulties in obtaining data at suitable spatial and temporal resolutions at a field site make full scale calibration and verification of linking equations implausible. Studies using physical scale models to calibrate and validate the performance of interaction points during flood flows are limited. Recently Russo et al. (2013) and Djordjević et al. (2013) investigated the hydraulic performance of gully pots, however they reported surface to sewer flow conditions only. Leandro et al. (2014), Lopes et al. (2015) and Martins et al. (2014) studied the hydrodynamic effects of the flow inside a gully without grate and proposed coefficients for the drainage flow. Bazin and Nakagawa (2014) quantified and modelled flow exchange between below and above ground systems but their tests were limited to scenarios with pressurised pipe conditions only and the scale of the model limited the range of flow Reynolds numbers tested. Fraga et al. (2015) validated a 1D-2D dual drainage model using a real-scale physical model to quantify rainfall-runoff transformation and presented a satisfactory performance (discrepancies were below 2%) of the numerical model when replicating water depth and discharge at several locations in a drainage network. However to date, no study has presented experimental validation of interaction flow modelling during unsteady tests featuring both surface to sewer and sewer to surface flow conditions.

To address this gap, this paper uses a physical model of a surface/pipe system linked via a scaled manhole to present experimental datasets of sewer-surface flow exchange. The tests conducted here are limited to conditions where no manhole lid is present, as may be the case where the lid has previously been removed or ejected due to surcharge. This conditions was chosen to enable a series of steady state experiments over a range of flow rates and exchange conditions are used to assess the applicability of weir and orifice equations to represent exchange flows as well as identify suitable discharge coefficients to represent energy losses. In order to validate these relationships in unsteady conditions, the functions are implemented within a Finite Volume (FV) Godunov-based numerical model, and its performance is compared to experimental datasets from a series of unsteady flow tests.

2. Overview of surface–subsurface linking equations

This section provides an overview of the weir and orifice linking equations which are commonly used to determine the exchange of flow at the interface within urban flood modelling.

2.1. Surface-to-sewer exchange

Considering an equivalent datum point, surface-to-sewer exchange through a linking node occurs in all cases when the hydraulic head of surface flow is greater than the hydraulic head of the pipe flow. Within coupled urban flood models (e.g. Chen et al., 2007; Djordjević et al., 2005; Leandro et al., 2009; Martins et al., 2016; Seyoum et al., 2012) this exchange flow is commonly quantified using equations originally derived for flow over a weir or through an orifice. When considering the surface elevation relative to the pipe flow hydraulic head (Z_{crest}), two conditions can be defined.

2.1.1. Head in the pipe network less than surface elevation

In this case, the free weir equation is normally used to describe flow exchange. Within urban flood models the length of the weir is taken as the manhole perimeter, and the hydraulic head of the flow is considered to be equal to the flow depth above the surface elevation (h_s), (i.e. velocity head is assumed to be negligible). Hence the linking equation is taken as:

$$-Q_e = \frac{2}{3} C_i \pi D_M (2g)^{1/2} (h_s)^{3/2} \tag{1}$$

where Q_e is flow exchange (m^3/s) and D_M is the manhole diameter (m), C_i is an energy loss coefficient that is included in order to account for losses due to viscous effects (–). Within existing flood models, the free weir scenario is considered applicable in all cases when pipe network hydraulic head does not exceed the surface elevation, although in Djordjević et al. (2005) it is noted that a somewhat reduced capacity should be considered at high flow rates when the manhole becomes submerged by the surface flow.

2.1.2. Head in the pipe network exceeds surface elevation

In this case, Chen et al. (2007) use a linkage based on a submerged weir equation, in which a term is included to account for the difference between surface flow depth and hydraulic head in the pipe network (h_p). This can be expressed as:

$$-Q_e = C_i \pi D_M (2g)^{1/2} (h_s)(h_s + Z_{crest} - h_p)^{1/2} \tag{2}$$

where Z_{crest} is the height difference from the invert of the pipe system to the level of the surface. This linkage is considered applicable when $h_p > Z_{crest}$ and $h_s < A_M/\pi D_M$ where A_M is manhole area (m^2). If $h_s > A_M/\pi D_M$ the link is considered fully submerged and the submerged orifice formula is expected to be a more suitable description of flow behaviour. The submerged orifice equation can be expressed to provide flow exchange as:

$$-Q_e = C_i A_M (2g)^{1/2} (h_s + Z_{crest} - h_p)^{1/2} \tag{3}$$

In this case, the discharge coefficient C_i accounts for energy losses due to flow through the orifice, the continued contraction of the jet as it passes through the restriction (vena contracta), and the assumption of negligible velocity head in the upstream (i.e. surface) flow.

2.2. Sewer-to-surface exchange

Considering an equivalent datum point, sewer-to-surface exchange through a linking node occurs when the total head in the pipe system is greater than the total head of the surface flow. Within flood models, flow exchange is commonly evaluated (Djordjević et al., 2005) by considering the interface point to act as an orifice. Considering surface velocity head to be negligible this can be expressed as:

$$Q_e = C_i A_M (2g)^{1/2} \left[h_p - (h_s + Z_{crest})\right]^{1/2} \quad (4)$$

Eq. (4) is also applicable in cases where $h_s = 0$.

2.3. Implementation with numerical models

The application of these equations is usually conditioned by the type of numerical model used. Decoupled models (Palla et al., 2016) do not simulate the sewer system and therefore limit the above to below ground exchange by defining a maximum sewer capacity. This implies a one cell per connection system and allows only drainage to be computed based upon a stage (surface depth) *vs* discharge relationship. The fact that these models do not account for surcharge is a limitation. Fully coupled models (Martins et al., 2016) compute both the surface and the sewer flow and link them using Eqs. (1)–(4), adding or subtracting the exchange flows or the volume of water to the surface and the sewer systems. Two main approaches can be identified, either time linking points can be defined at each time-step (Borsche and Klar, 2014) or the models can be interleaved (Martins et al., 2016). Similar discretisations and numerical models for sewer and surface can use time linking approaches whilst different models usually require interleaving and imply an asynchronous connection with different time steps for each model. For both options surface and sewer flows are modelled as independent systems and the interaction is performed at the end of each time-step. This numerical interaction is controlled by Eqs. (1)–(4) making use of the head in the manhole, obtained from the numerical sewer simulation by considering the total head inside of the manhole node as the sewer head, and the surface head obtained from the cell or node on top of the manhole crest, along with the empirical discharge coefficient. It is therefore of importance that the discharge coefficients are well defined. As the surface and sewer systems are modelled independently, the local effects of sewer surcharge or free surface effects on the surface flow depth are only considered in the next time-step. In addition the direct feedback effects of the exchange flow on the surface and sewer hydraulic head is only considered in terms of net flow rates, i.e. flow depths are calculated without consideration of local shock or acceleration effects around the drainage structure caused by the exchange itself. This differs from the physical reality were the interaction flows affect local hydrodynamics around the exchange point. Due to the sensitivity of the flow exchange to the relative head calculation, the impact of local hydrodynamics around the exchange node and the definition of representative head in the surface and sewer systems may have a significant effect on the flow exchange and the modelling results. These aspects, which are included within the quantification of discharge coefficients, should hence be considered when evaluating the effectiveness of the linking equations.

3. Methodology

This section describes the experimental and numerical approaches used to achieve the objectives stated in Section 1.

3.1. Experimental setup

The experimental facility consists of a physical model of sewer pipe with no slope connected via a manhole to a shallow flow flume (Rubinato, 2015; Rubinato et al., 2013). The sewer pipe has an internal diameter of 75 mm and the circular manhole has the internal diameter of 240 mm (Fig. 1).

The pipe and manhole are constructed based on a 1/6 geometrical scale of a typical UK urban drainage system. The flume bed (slope 0.001) is aligned with the top of the manhole and is 4 (m) wide and 8 (m) long. The bed of the flume is 0.478 (m) above the invert level of the pipe. The facility (pipe and flume) is constructed from PVC, based on experimental stage/discharge measurements the Manning's roughness coefficient of the flume surface is quantified to be 0.009 ($s\,m^{-1/3}$). This facility allows shallow flow over the surface which interacts with the sewer flow via the manhole (Fig. 1). Inlet flows to the pipes and the surface can be controlled in real time by automated valves controlled via Labview™ software, allowing both steady flows and unsteady storm profiles to be simulated. Flow into and out of the above and below ground systems are continuously monitored by electromagnetic flowmetres (Q_1, Q_2, Q_3, Q_4). The accuracy of the flowmetres has been validated using volumetric discharge readings using the laboratory measurement tank.

Calibrated pressure transducers (manufactured by GEMS instruments) within pipe invert and the bed of the flume are used to determine pressure and flow depth in the sewer and on the surface respectively. P_{sewer} and $P_{surface}$ are located respectively 350 mm and 460 mm from the centre of the manhole (Fig. 2). Transducers were calibrated such that transducer output signal (mA) can be directly related to gauge pressure. This step was completed using a pointer gauge with an averaged recorded error between mea-

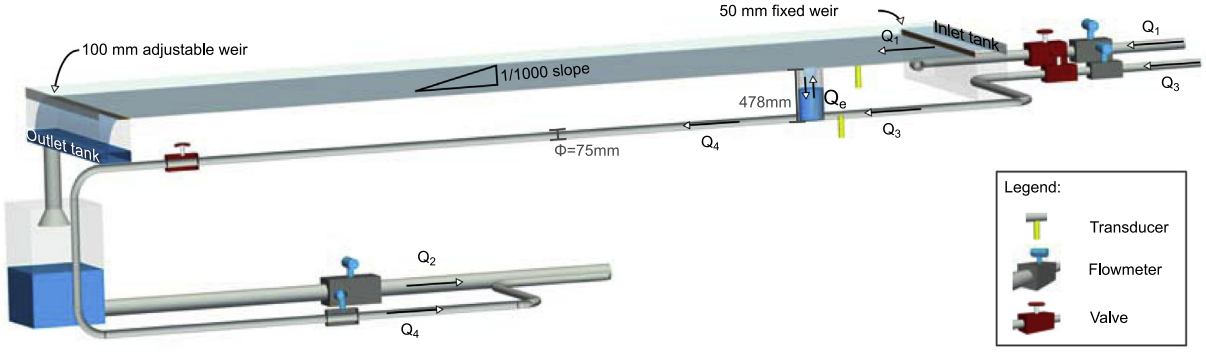

Fig. 1. Longitudinal profile of the model (not to scale, lengths in mm). Q_1 = surface inflow, Q_2, = surface outflow, Q_3, = sewer inflow, Q_4 = sewer outflow, Q_e = flow exchange from sewer-to-surface.

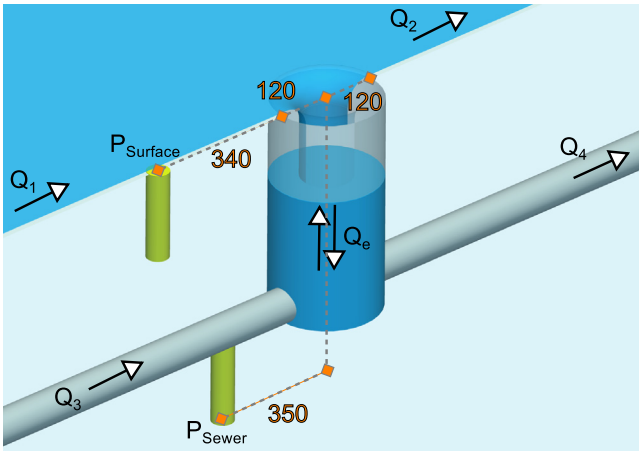

Fig. 2. Location of the pressure measurement points (distances in mm) around the manhole.

sured values and defined calibration relationships quantified to be ±0.109 (mm) within the range of measurement for $P_{surface}$ (range of water depth 0–100 mm), ±0.72 (mm) within the range of measurement for P_{sewer} (range of water depth 0–600 mm). All pressure transducers are linked to Labview software such that readings from the facility instrumentation are logged against time.

3.1.1. Configuration of steady state tests

To evaluate the applicability of the weir and orifice equations to describe flow exchange and to identify suitable range for discharge coefficients under steady state flow conditions, a series of tests have been conducted using the experimental facility described in Section 3.1. Tests were conducted by varying the inflows to the pipe and surface systems (as appropriate) and recording the resulting flow exchange and pressure head measurements. The test conducted can be classified into four exchange scenarios (S) as follows (Fig. 3).

S1 *Inflow into non-surcharged sewer*; Flow on the surface with no flow in the sewer system. Flow exchange from the surface to the sewer system;
S2 *Inflow into surcharged sewer*; Flow on the surface and in the sewer system, with hydraulic head in the sewer (h_p) greater than Z_{crest} but less than the surface flow depth (h_s). Flow exchange from the surface to the sewer system.
S3 *Outflow over wet floodplain*; Flow on the surface and in the sewer system, with hydraulic head in the sewer system (h_p) greater than the the surface flow depth (h_s). Flow exchange from the sewer system to the surface.
S4 *Outflow over dry floodplain*; Flow in the sewer system with no flow on the surface ($h_s = 0$), with hydraulic head in the pipe network (h_p) greater than Z_{crest}. Flow exchange from the sewer system to the surface.

Steady state flow exchange rate (Q_e) is quantified based on mass conservation principles and sewer flow measurements:

$$Q_e = \overline{Q_3} - \overline{Q_4} \tag{5}$$

where $\overline{Q_3}$ and $\overline{Q_4}$ is the time-averaged sewer inflow and outflow respectively. Surface depth, h_s was evaluated via a temporal average of pressure readings at $P_{surface}$. In this location measurements were neither affected by the hydraulic-jump region in surcharging conditions nor by the descending free surface profile in surface-to-sewer conditions. h_p is evaluated via a temporal average of the pressure reading at P_{sewer}.

For all steady state tests, flows were first established and allowed to stabilise before data values were recorded. Once established, data were collected for a period of five minutes in order to define reliable temporally averaged values.

3.1.2. Experimental flow exchange error analysis

The error in experimentally measured steady flow exchange can be defined as flow meter instrumentation error plus error due to any water volume (V) change within the experimental facility during each test (dV/dt). Assuming that sufficient temporal averaging of flow data is performed, dV/dt is assumed to be negligible. In order to estimate the instrumentation error, a parameter (ξ) is defined for each test based on the difference between Eq. (5) and the flow exchange calculated using the flow meters characterising the floodplain inlet ($Q_{In} = \overline{Q_1} + \overline{Q_3}$) and outlet flows ($Q_{Out} = \overline{Q_2} + \overline{Q_4}$), normalised by the total inflow (Q_{In}) and scaled by the flow exchange (Q_e):

$$\xi_f = (Q_{Out} - Q_{In})\frac{Q_e}{Q_{In}} \tag{6}$$

where $\overline{Q_1}$ and $\overline{Q_2}$ are the time-averaged surface inflows and outflows respectively.

3.1.3. Configuration of Time-Varying (unsteady) tests

In order to understand the performance of the discharge linking equations within unsteady flow conditions a series of additional tests were conducted. Nine unsteady flow tests were simulated within the experimental facility in which surface inflow (Q_1) was maintained constant (8.15 l/s) whilst a flood hydrograph run through the sewer pipe, such that surface-to-sewer and sewer-to-surface exchange occurs during each test. Sewer inflow hydrographs were introduced via the control of a calibrated sewer pipe inflow valve automated via Labview™ software (Rubinato, 2015). All unsteady tests had a minimum total duration of 6 min. Pressure and flow readings within the facility were recorded in real time over the duration of each test. To examine a range of hydraulic complexities, tests with a single peak in sewer surcharge were simulated (Fig. 4) featuring a range of surcharge durations and the maximum surcharge rate, quantified in terms of Q_{3max}/Q_1. Key characteristics of each of the time varying test events tests are presented in Table 1.

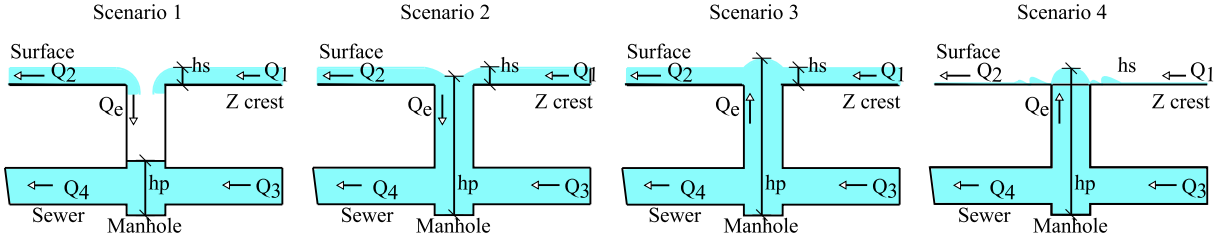

Fig. 3. Hydraulic scenarios tested within the experimental facility – S1, S2, S3, S4.

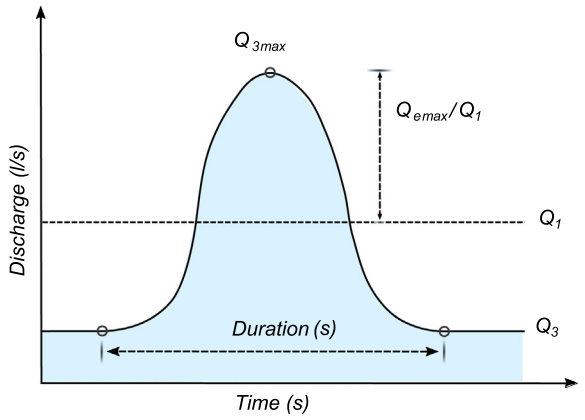

Fig. 4. Diagram of key parameters listed in Table 1 for a single peak event.

Table 1
Time varying test characteristics.

$Q_1 = 8.15$l/s		
Test ID.	Q_{3max}/Q_1	Duration (s)
T1	0.65	41
T2	0.66	66
T3	0.68	131
T4	0.96	67
T5	0.97	102
T6	0.98	201
T7	1.26	102
T8	1.26	197
T9	1.26	341

Experimental quantification of the instantaneous value of flow exchange against time during each event was not feasible due to the unsteady variation of mass over each test (although examination of the measured mass balance can provide an illustrative indication of flow exchange). Therefore to examine the performance of both the linking Eqs. (1)–(4) and the experimentally derived coefficients in unsteady flow conditions, a series of numerical simulations were conducted.

3.2. Numerical flood model

Floodplain flow is usually modelled by the depth-averaged 2D shallow water equations (SWE). 2D numerical modeling using the SWE has been extensively researched (see for example Ata et al., 2013; Liang and Marche, 2009; Song et al., 2011; Kesserwani and Wang, 2014). The SWE can be obtained by depth-integrating the three-dimensional Reynolds-Averaged Navier–Stokes equations, neglecting the vertical acceleration term and assuming the pressure distribution to be hydrostatic. The assumptions are that the vertical dimension is smaller than the horizontal one and that the streamlines remain approximately parallel to each other. In a conservative matrix form, the SWE including sewer source term read:

$$\partial_t \mathbf{U} + \partial_x \mathbf{F}(\mathbf{U}) + \partial_y \mathbf{G}(\mathbf{U}) = \mathbf{S}(\mathbf{U}) \tag{7}$$

In (7), (x, y) are the spatial Cartesian coordinates and t is time. $\mathbf{U}$ is the vector containing the flow variables, and $\mathbf{F}(\mathbf{U})$ and $\mathbf{G}(\mathbf{U})$ are the Cartesian components of the flux vectors. $\mathbf{S}(\mathbf{U})$ is the vector of source terms that, can be decomposed into $\mathbf{S}(\mathbf{U}) = \mathbf{S_s} + \mathbf{S_b} + \mathbf{S_f}$:

$$\mathbf{U} = \begin{pmatrix} h \\ hu \\ hv \end{pmatrix}, \mathbf{F} = \begin{pmatrix} hu \\ hu^2 + \frac{1}{2}gh^2 \\ huv \end{pmatrix}, \mathbf{G} = \begin{pmatrix} hv \\ huv \\ hv^2 + \frac{1}{2}gh^2 \end{pmatrix} \tag{8}$$

$$\mathbf{S_b} = -gh\begin{pmatrix} 0 \\ \partial_x z_x \\ \partial_y z_y \end{pmatrix}, \mathbf{S_f} = -C_f \begin{pmatrix} 0 \\ u||\vec{u}|| \\ v||\vec{u}|| \end{pmatrix}, \mathbf{S_s} = V_s \begin{pmatrix} 1 \\ -u_{bed} \\ -v_{bed} \end{pmatrix} \tag{9}$$

In (8) and (9), g (m s^{-2}) is the constant gravitational acceleration; h (m) is the water depth, hu and hv (m^2 s^{-1}) are the unit-width discharge expressed in terms of the velocity $\vec{u}$ Cartesian components u and v (m s^{-1}). $\mathbf{S_b}$ and $\mathbf{S_f}$ are, respectively, the topography and friction slope terms involved in the momentum equations with $C_f = gn^2h^{-1/3}$ (n being the Manning roughness coefficient). $\mathbf{S_s}$ denotes a sewer flux term involved in the continuity equation in terms of vertical velocity V_s, which represents a source added uniformly or a sink term removed proportionally to the water depth; whereas u_{bed} and v_{bed} are the local horizontal velocities at the bed level, assumed zero during the numerical tests.

The system (7) is solved using the first order in space and time finite volume method (Martins et al., 2015). The domain discretisation is based on a 2D unstructured node-centred triangular mesh. The numerical integration of the equations is done with the equations in their integral form and is divided into two steps, the space integral and the time integral. For the space integral, using Gauss divergence theorem the area integral is changed to a curve integral that accounts for the fluxes over the boundaries of the cell. The inter-cell fluxes (ϕ_{hw}) are then evaluated through the use of a one dimensional Riemann problem between two generic adjacent points h and w (i.e a Roe Approximate Riemann solver). Boundary fluxes (ϕ_{hw}^{Out}) are calculated and updated as Dirichlet boundaries with a physical limiter for internal boundary conditions to avoid negative depths (i.e. a boundary cell cannot lose more water than it holds):

$$Q_e = \max\left(-\frac{\sum_{i=1}^{n} h_i A_i}{\Delta t}, Q_e\right) \tag{10}$$

where Q_e is the exchange flow calculated at the time step, h_i the depth of the cell on top of the manhole and A_i the area of the cell. The bed elevation source term (ψ_{hw}) is calculated using an upwind scheme, that avoids non-physical oscillations, derived respecting the extended C-property by projecting the source term onto the eigenvectors of the flux Jacobian. After the linearisation of the source term it is evaluated at the same state as the inter-cell fluxes. Bed friction source term is calculated outside the fluxes with a semi implicit Runge–Kutta-based point-wise scheme (Liang and Marche, 2009), whilst the discharge term is computed using an explicit point-wise scheme. The Wet-Dry front is treated using (Leandro et al., 2014) approach that avoids localised "negative depths", formulated to the SWE. The discretised form (7) becomes:

$$\mathbf{U}_\mathbf{h}^{n+1} = \mathbf{U}_\mathbf{h}^{n} + \frac{\Delta t}{A_h}\left(\sum_{\forall w \in Kn_h} \psi_{hw} - \sum_{\forall w \in Kn_h} \phi_{hw} - \sum_{\forall w \in Kn_h} \phi_{hw}^{Out}\right) + (\mathbf{S_f}(\mathbf{U_h}))_h^n + (\mathbf{S_s}(\mathbf{U_h}))_h^n \tag{11}$$

where h is the generic point to be evaluated, w is an adjacent neighbour point, Kn_h is the set of neighbour points of h, A_h is the computational area of point h, $\phi_{hw}, \phi_{hw}^{Out}$ and ψ_{hw} are the numerical fluxes evaluated using the Roe solver (Martins et al., 2015). Δt is evaluated using the equation:

$$\Delta t = CFL\frac{\Delta r}{\sqrt{u^2 + v^2} + \sqrt{gh}} \tag{12}$$

where the CFL coefficient is 1 and Δr is the distance between the computational cell centre and the computational cell edge.

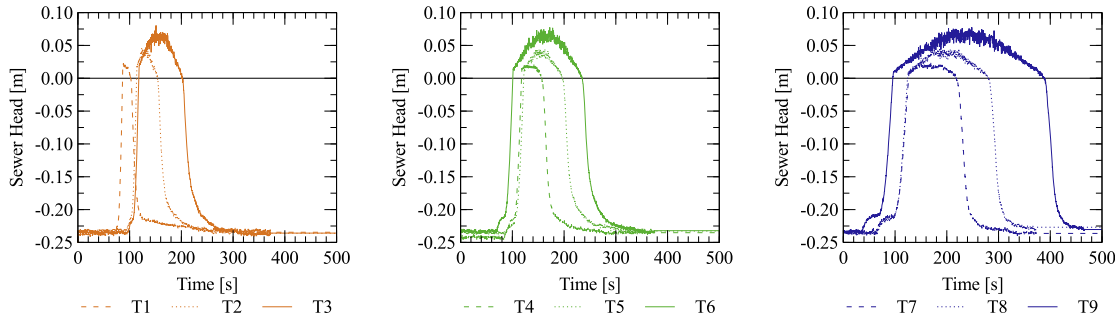

Fig. 5. Head used as internal boundary condition the numerical model through Eqs. (1)–(4) for computing the exchange. Zero refers to the crest elevation. T1-T9 indicate the ID for each unsteady test as displayed in Table 1.

The mesh size was computed using a length of 0.0125 (m) near the manhole crest increasing up to 0.2 (m) in the external boundaries (Schöberl, 1997) resulting in 11,186 computational cells.

3.2.1. Numerical model configuration

Steady state numerical simulations were conducted in order to confirm the validity of the numerical approach. Numerically calibrated discharge coefficients were obtained using principles described in Section 2 and compared to values obtained via experimental data. For each simulation sewer pipe pressure (Fig. 5) and and flow exchange were taken as measured in the experimental facility. To explore the sensitivity of the numerical simulations to variations in the selection of surface flow depth (as discussed in Section 3.1.1), a number of surface depth cases were tested for each simulation.

1. Numerical depth [$H_{P_{Surface}}$] – The surface depth used as h_s is the depth at the positions of the transducer $P_{Surface}$ obtained from the steady numerical results: $h_s = h_{P_{Surface}}$
2. Uniform depth [$H_{Manning}$] – An undisturbed uniform flow equal to the outlet flow is assumed at the surface. The depth is calculated using the Manning equation: $h_s = Q_1/(R_{h_s}^{2/3} S^{1/2} nb)$
3. Manhole depth [$H_{\overline{Mho}}$] – Using the previous numerical simulations the depth is established as the average of the depths obtained above the manhole considering the exchanges: $h_s = \overline{h_P} \forall P \in (x - x_0)^2 + (y + y_0)^2 < r_{Mho}^2$

For the steady state tests the boundary conditions used were:

- Free overfall weir (i.e critical depth in the vicinity of the manhole) for S1
- Eq. (5) for the internal boundary condition in the manhole for S2 and S3 based on the appropriate exchange sign

Following validation in steady conditions, the unsteady flow events described in Section 3.1.3 were simulated and results are used to examine the performance of the linking questions in unsteady flows. For these tests a similar configuration is applied to that of the steady state tests with the exception that the flow exchange is calculated through Eqs. (1)–(4) (using the coefficients derived from steady state tests), and the sewer head evaluated from the pressure transducer (P_{sewer}) at each timestep after a reduction to a 4 (Hz) sampling rate by averaging over six values.

4. Results and discussion

This section presents measured flow exchange and hydraulic head for each of the tests conducted over the four steady state flow scenarios S1, S2, S3 and S4. The performance of the linking Eqs. (1)–(4) is analysed and calibrated steady state coefficients are produced. Discharge coefficients are then compared to those obtained from steady state numerical simulations and the sensitivity to the surface head boundary conditions are examined. Finally, numerical simulations of the unsteady flow events are presented. The performance of the numerical model in unsteady state conditions is analysed based on: 1) comparisons of numerical simulated Q_e and measured ($Q_3 - Q_4$) flow exchange between surface and pipe systems over each event and 2) through averaged experimental outflow mass balance exchange rate ($\overline{Q}_3 - \overline{Q}_4$) against averaged numerically simulated $\overline{Q}_e$ monitored over each test.

4.1. Steady state results for the calibration of linking equations

Table 2 displays time averaged flow exchange and relative surface/pipe head measurements taken during the steady state tests as described in Section 3. In addition, to facilitate use of findings at larger geometrical scales, several non-dimensional parameters are presented. These include standard surface flow Froude number (Fr_s) and pipe flow Reynolds number (Re_p), Reynolds number of the flow through the manhole (Re_m) (where characteristic velocity is based on flow exchange, Q_e and manhole area, and characteristic length scale is taken as the diameter of the manhole) as well as the geometrical scaling parameter based on the ratio of surface flow depth to manhole diameter.

The maximum inflow rate for both surface (Q_1) and sewer (Q_3) systems was 11 (l/s). Based on a geometrical scale of 1 to 6, this flow rate corresponds to approximately 70 (l/s) in a full scale pipe system based on Reynolds similitude. Velocities on the surface are quantified to be between 0.1 and 0.25 (m/s) for the tests reported here, with flow depths between 77 mm and 191 mm. Surface flow Froude numbers are in the range 0.151–0.691, and are hence subcritical. Based on Froude numbers similitude this corresponds to a real scaled velocity range of 0.245 and 0.625 (m/s).

Figs. 6–9 show measured flow exchange rate (Eq. 6) against the terms of the relevant linking Eqs. (1)–(4) as described in Section 2 for each correspondent scenario (S1, S2, S3 and S4). In Figs. 6–9 error bars are based on the error parameter ξ_f [Eq. (6)] for each test. Trend lines are plotted considering minimum, expected and maximum values of Q_e based on this range.

4.1.1. S1 results

Fig. 6 presents the observed surface-to-sewer flow exchange against the predictions of the weir Eq. (1) for all tests conducted under S1.

Flow exchange can be observed to increase proportionally to $h_s^{3/2}$, as is consistently predicted by the free weir Eq. (1). This relation is shown to be valid up to the depth $0.062D_M$ (the maximum tested).

Table 2
Experimental measured data including flow exchange Q_e (l/s), flow exchange variation (l/s), surface flow depth h_s (m), pipe network head h_p (m) and calculated non-dimensional parameters inclusive of surface Froude number Fr_s, scaled flow depth h_s/D_M, Reynolds number in both pipe Re_p and manhole Re_M obtained from steady state tests – S1, S2, S3 and S4.

	Flow exchange Q_e (l/s)	Percentage surcharge (%) $[(Q_3 - Q_4)/Q_3]$	Flow exchange variation eq.(6) ξ_f (l/s)	Surface flow depth h_s(m)	Pipe network head h_p (m)	Surface Froude Fr_s (–)	Scaled flow depth h_s/D_M (–)	Pipe Reynolds Re_p(–)	Manhole Reynolds Re_m(–)
S1	0.69	–	0.0056	0.0077	–	0.666	0.032	11616	3630
	0.77	–	0.0152	0.0082	–	0.672	0.034	13024	4070
	0.83	–	0.0216	0.0085	–	0.667	0.035	14024	4382
	0.88	–	0.0235	0.0088	–	0.674	0.037	14915	4661
	0.90	–	0.0251	0.0090	–	0.675	0.038	15304	4782
	0.93	–	0.0255	0.0092	–	0.672	0.038	15795	4936
	0.97	–	0.0330	0.0094	–	0.674	0.049	16493	5154
	1.06	–	0.0400	0.0097	–	0.685	0.040	17992	5622
	1.09	–	0.0425	0.0099	–	0.683	0.041	18574	6804
	1.11	–	0.0401	0.0100	–	0.684	0.042	18773	5867
	1.14	–	0.0413	0.0102	–	0.689	0.042	19247	6015
	1.15	–	0.0507	0.0104	–	0.691	0.043	19414	6067
	1.20	–	0.0536	0.0107	–	0.687	0.044	20585	6433
	1.21	–	0.0528	0.0108	–	0.687	0.045	20363	6363
	1.25	–	0.0557	0.0110	–	0.691	0.046	21140	6606
S2	0.24	−2.55	0.0061	0.0099	0.478	0.458	0.041	161675	1258
	0.25	−2.65	0.0067	0.0114	0.480	0.455	0.047	161865	1308
	0.28	−3.02	0.0076	0.0126	0.481	0.460	0.052	162297	1487
	0.30	−3.19	0.0086	0.0135	0.482	0.472	0.056	162615	1570
	0.32	−3.4	0.0074	0.0148	0.484	0.472	0.062	162939	1675
S3	1.73	25.08	0.032	0.0160	0.510	0.364	0.077	87359	9137
	2.27	30.24	0.046	0.0167	0.515	0.340	0.070	88764	12022
	2.77	34.30	0.082	0.0173	0.520	0.322	0.072	89813	14651
	3.13	36.79	0.111	0.0178	0.525	0.311	0.074	91013	16556
	3.48	38.98	0.105	0.0182	0.529	0.300	0.076	92344	18437
	3.84	41.38	0.126	0.0185	0.533	0.292	0.077	92030	20301
	4.12	43.03	0.139	0.0188	0.536	0.285	0.078	92399	21809
	4.27	43.52	0.617	0.0191	0.538	0.280	0.079	93748	22577
S4	1.74	25.18	0.090	–	0.506	0.234	0.040	87465	9200
	2.31	30.55	0.027	–	0.513	0.207	0.043	88952	12226
	2.75	34.12	0.015	–	0.519	0.190	0.046	89791	14534
	3.18	37.38	0.004	–	0.524	0.177	0.048	90130	16812
	3.57	39.85	0.023	–	0.528	0.167	0.050	91168	18874
	3.82	41.24	0.037	–	0.532	0.160	0.051	92243	20232
	4.10	42.80	0.051	–	0.536	0.156	0.052	92830	21711
	4.30	43.80	0.056	–	0.539	0.151	0.053	93366	22735

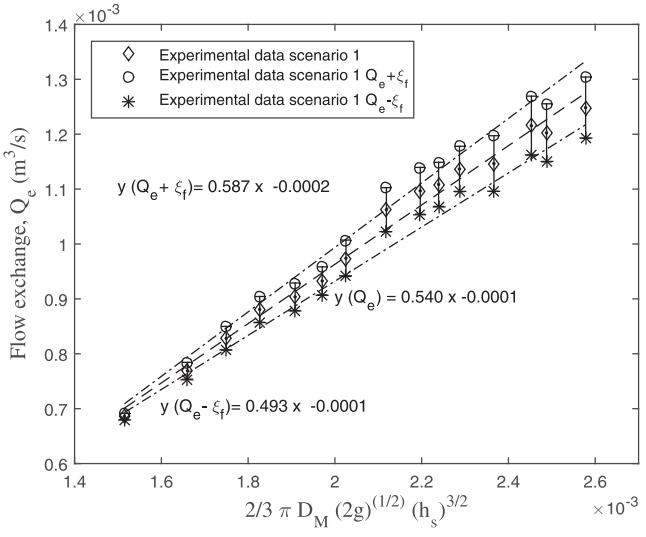

Fig. 6. Plot of flow exchange (Q_e) against the weir equation for S1. Trend lines based on calibrated weir equation considering $Q_e, Q_e + \xi_f, Q_e - \xi_f$.

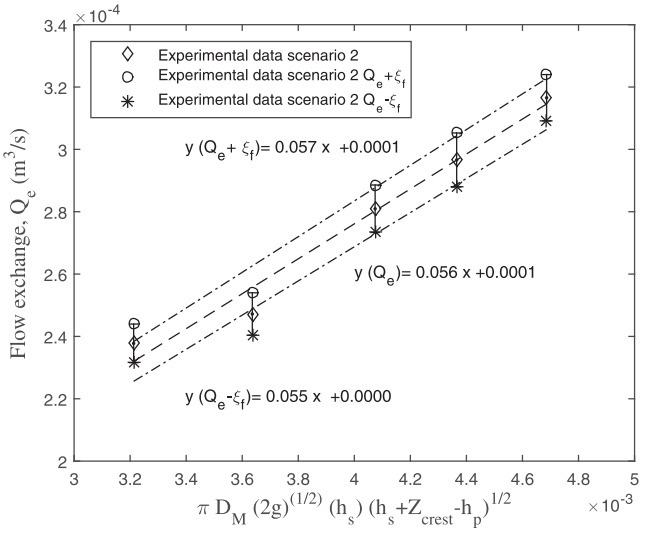

Fig. 7. Plot of flow exchange (Q_e) against governing head differential ($h_s - h_p$) for S2. Trend lines based on calibrated submerged equation considering $Q_e, Q_e + \xi_f, Q_e - \xi_f$.

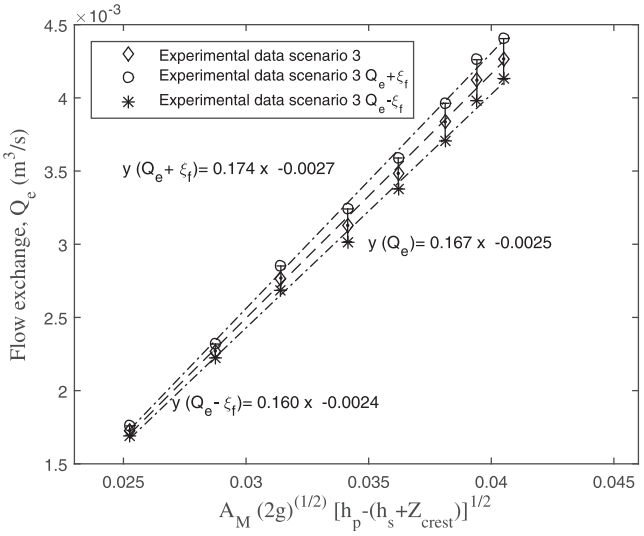

Fig. 8. Plot of flow exchange (Q_e) against the terms of the orifice equation for S3. Trend lines based on calibrated orifice equation considering $Q_e, Q_e + \xi, Q_e - \xi$.

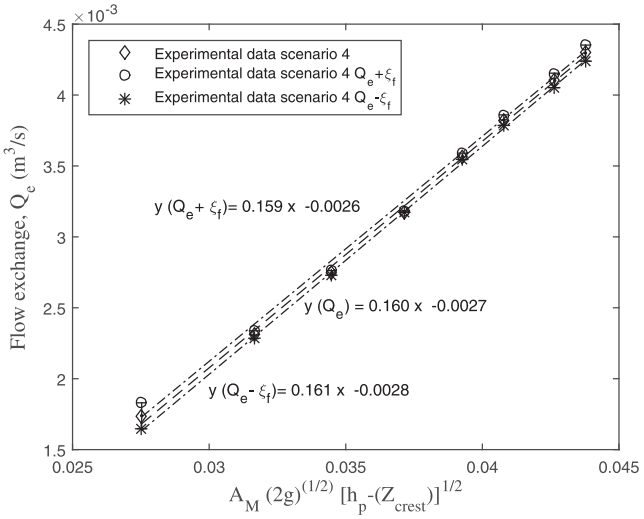

Fig. 9. Plot of flow exchange (Q_e) against the terms of the orifice equation for S4. Trend lines based on calibrated orifice equation considering $Q_e, Q_e + \xi, Q_e - \xi$.

In this region, calibrating the free weir equation (as shown) against the experimental results provides a discharge coefficient in the range 0.493 to 0.587, based on the potential experimental error.

4.1.2. S2 results

For the tests conducted under S2, the pipe flow conditions were set to 9.3 l/s (Table 2), in order to limit the capacity of the sewer system to receive water from the above ground system. Five surface inflow conditions (Q_1) were tested in the above ground system to evaluate different values of h_s. In all cases $h_s > h_p$ resulting in surface-to-sewer exchange. Fig. 7 presents observed surface-to-sewer flow exchange against the terms of the submerged weir Eq. (2) for all tests conducted in S2.

In all cases tested, the presence of sewer network flow caused the manhole to be visibly submerged/drowned. Fig. 7 shows the dependency of measured flow exchange on the head difference between surface and sewer flow. For the range tested, calibrating the submerged weir equation against the experimental results provides a range for the discharge coefficient between 0.054 and 0.057, based on the potential experimental error.

4.1.3. S3–S4 results

Fig. 8 and 9 present observed surface-to-sewer flow exchange against the terms of the orifice Eq. (4) for all tests conducted in S3 and S4.

Flow exchange is observed to increase with head difference between pipe and surface systems (Fig. 8 and 9). The calibration of the orifice equation against the experimental results provides a range for discharge coefficient between 0.159 and 0.174 for S3 and between 0.159 and 0.161 for S4.

4.2. Discharge coefficients

Table 3 presents the coefficients obtained for both the experimental (expected, upper and lower bound based on the assessment of the experimental error as described in Section 3.1.2) and and numerical simulations (using the three depth conditions described in Section 3.2.1), together with a goodness of fit parameter R^2 for each relationship. Numerically obtained coefficients are slightly lower than the experimental values, although they are within the experimental range of steady state flows. In S1 the numerically generated coefficients were within the range of the experimental derived values, irrespective of the surface flow depth option used. Whilst the numerical coefficients for S2 overestimate the experimental values, this can be attributed to the very small head difference between the sewer system and the surface for this scenario. The low exchange flows in this scenario make the resulting errors less relevant. For S3 and S4 the numerical coefficients are within the experimental range of the experimentally derived values with the exception of the scheme using $H_{\overline{Mho}}$ (which is slightly above experimental values). This difference can be attributed to the fact that the head on top of the manhole is always above the free water surface in an orifice discharge situation, and hence a lower head differential is obtained. However, overall all the numerical simulation results a linear fit between flow exchange and the the weir/orifice linking equations (the lowest R^2 is 0.911).

4.3. Discussion of steady state tests

The empirical results and R^2 values presented in Section 4.3 show that as long as the prevailing surface and sewer flow conditions are identified correctly, the existing modelling framework comprising of weir and or orifice equations described in Section 2 with a constant discharge coefficient can provide a suitable description of the linkage between pipe and surface flows in steady state conditions. However, the calibrated weir discharge coefficients derived in this study differ from studies of classical weirs (Reda et al., 2011; Bautista-Capetillo et al., 2013; Lee et al., 2012; Massey et al., 1998), whilst no comparable discharge coefficients in the orifice flow regime were found in the literature. This suggests that modelling studies using uncalibrated discharge coefficients, or those based on conventional weirs and orifices, may have high uncertainty associated with flows through above/below ground linking nodes. This uncertainty is associated with complex geometries within urban drainage hydraulic structures. These geometries bring additional head losses that are not taken into account when 'standard' weir/orifice discharge coefficients are used. This is especially the case for sewer-to-surface exchange, as flow discharging to the surface may lose a significant amount of energy via turbulence in the manhole structure as well as through the orifice. It is suggested that the coefficients presented in this study provide the closest current approximation to urban flood interaction head losses in the case of flow via a cylindrical manhole

Table 3
Experimentally and numerically obtained discharge coefficients for weir and orifice equations [(1)–(4)] identified from steady state tests (S1 to S4) and correlation coefficient for each datasets.

Scenario		Equation utilized	Experimental			Numerical		
			Lower (based on $Q_e - \xi$)	Expected (based on Q_e)	Upper (based on $Q_e+\xi$)	$H_{P_{Surface}}$	$H_{Manning}$	$H_{\overline{Mho}}$
C_i	S1 weir	(1)	0.493	0.540	0.587	0.516	0.492	
	S2 submerged weir	(2)	0.055	0.056	0.057	0.095	0.077	0.110
	S3 orifice	(4)	0.160	0.167	0.174	0.172	0.168	0.205
	S4 orifice	(4)	0.159	0.160	0.161	0.160	0.160	0.191
R^2	S1 weir	(1)	0.987	0.988	0.988	0.989	0.986	
	S2 submerged weir	(2)	0.973	0.975	0.976	0.970	0.979	0.911
	S3 orifice	(4)	0.998	0.998	0.998	0.998	0.998	0.997
	S4 orifice	(4)	0.995	0.998	1	0.998	0.998	0.999

with no lid. Although it is also recognised that further work needed to fully elucidate the relationship between manhole geometry, flow rates and energy losses in surcharge/free drainage conditions including the effects of different manhole lids, as well as hydraulic conditions outside the range of the tests conducted here. In particular interaction flows may behave differently under; 1. very low flow depths (such as runoff flows) where the full weir length/orifice areas may not be utilised and 2. super-critical surface flow conditions which may invalidate the velocity head assumption of the weir Eq. (1) when simulating surface to sewer flow conditions.

4.4. Time varying tests and model validation

The calibrated steady state head/flow exchange relationships were integrated into the numerical model described in Section 3.2. The numerical model was used to replicate the nine time-varying tests as described in Section 3.1.3. In order to assess the sensitivity of the simulations to surface flow depth selection and variability in discharge coefficients caused by the experimental error defined in Eq. (6), each simulation was run using the different surface depth conditions described in 3.2.1 as well as for the lower bound, expected and upper bound coefficients identified in the steady state experiments (Table 3). Numerical simulations were run for a duration of 500 s for all three surface conditions combined with the three experimental coefficients for all unsteady cases.

Numerical simulations were analysed in terms of flow exchange hydrographs and validated against the experimental results via comparison of averaged measured exchange rate ($\overline{Q_3Q_4}$) against averaged numerically simulated Q_e over each test.

4.4.1. Flow exchange hydrographs

The numerical exchange vs time for all the events tested is presented in Fig. 10. The instantaneous value of $Q_3 - Q_4$ (i.e. time lagged experimentally measured Q_e) is also plotted for comparison. Since the exchange is computed using the measured sewer pressure data, rapid oscillations are present in the exchange values for all the tests as expected. All numerical simulations overestimate surcharge flows and underestimate drainage flows during each event. Also numerical simulations do not capture the experimental flow oscillation (peak flow for each event displayed in Fig. 5) which is observed to occur at the end of each surcharge event, which is attributed to the suction effect. In terms of absolute values upper coefficient $H_{\overline{Mho}}$ values are usually below lower coefficient $H_{P_{Surface}}$ values and $H_{Manning}$ for the orifice and free weir conditions whilst for the submerged orifice conditions $H_{P_{Surface}}$ is highest. It also should be noted that whilst for the behaviour on the ascending branch for the $H_{P_{Surface}}$ and $H_{Manning}$ is very similar, for the descending branch $H_{Manning}$ has a closer behaviour to $H_{\overline{Mho}}$. This behaviour is in fact the only time where some difference in the shape of the instantaneous exchange values can be observed between all of the numerical unsteady simulations. In the descending branch, $H_{P_{Surface}}$ tends to produce a surface-to-sewer discharge peak whilst $H_{\overline{Mho}}$ and $H_{Manning}$ tend to have a smoother, more stable behaviour. The largest shape differences occur in the transition from orifice to submerged orifice and from submerged orifice to free weir. At the peak exchange, the difference between the maximum and the minimum flow rates can reach 3.5 l/s showing a high sensitivity to both the discharge coefficients and the surface head used.

4.4.2. Outflow mass balance

For the unsteady experimental and numerical results the averaged exchange rate was quantified. The values for each of the numerical result are presented against the respective experimental values in Fig. 11. Bigger markers represent bigger $Q_{e_{max}}/Q_1$ ratios and the marker colouring is related to the peak duration as presented in Table 1. Globally, the numerical simulations overestimate the average exchange discharge for every event tested. Hence the simulations either underestimate surcharge flows or overestimate drainage flows, or show both of these effects. The results show a closer agreement when using the $H_{\overline{Mho}}$ as the surface flow depth for longer duration peaks whilst for shorter duration peaks $H_{P_{Surface}}$ and $H_{Manning}$ surface depths are closer to the experimental values. Global differences between experimental and numerical values range from 0.35 l/s to 2.35 l/s. Lower bound discharge coefficients provide the closest agreement between numerical (using $H_{P_{Surface}}$) and experimental results as shown in T1, whilst the larger differences are associated with the upper bound coefficients (using $H_{P_{Surface}}$) as displayed for T9. Average differences for each numerical test are 0.94, 0.91 and 0.71 for the $H_{P_{Surface}}$, $H_{Manning}$, and $H_{\overline{Mho}}$ respectively. $H_{P_{Surface}}$ and $H_{Manning}$ present very similar results due to Eq. (10) prescribing the maximum amount of water that can leave the domain through the manhole. This limiter was imposed in order to avoid negative depths on top of the manhole as mentioned in Section 3.2.

4.4.3. Discussion of unsteady tests

When tested in unsteady conditions the results confirm that the numerical model tends to overestimate the discharge when using the experimentally derived coefficients. Due to the accuracy of the models observed in steady state conditions, this suggests that additional uncertainties are introduced from the modelling approach caused by the unsteady nature of the flow and the aggregation at the interaction node. Fig. 10 suggests that the overestimation of surcharge flows is the most significant discrepancy between experimental and numerical observations for most events. This suggests that in unsteady surcharging flow conditions, significant additional head losses are encountered over and above those in steady state flows.

The model using $H_{\overline{Mho}}$ provided a better overall agreement with the experimental observations, likely due to this scheme's use of a

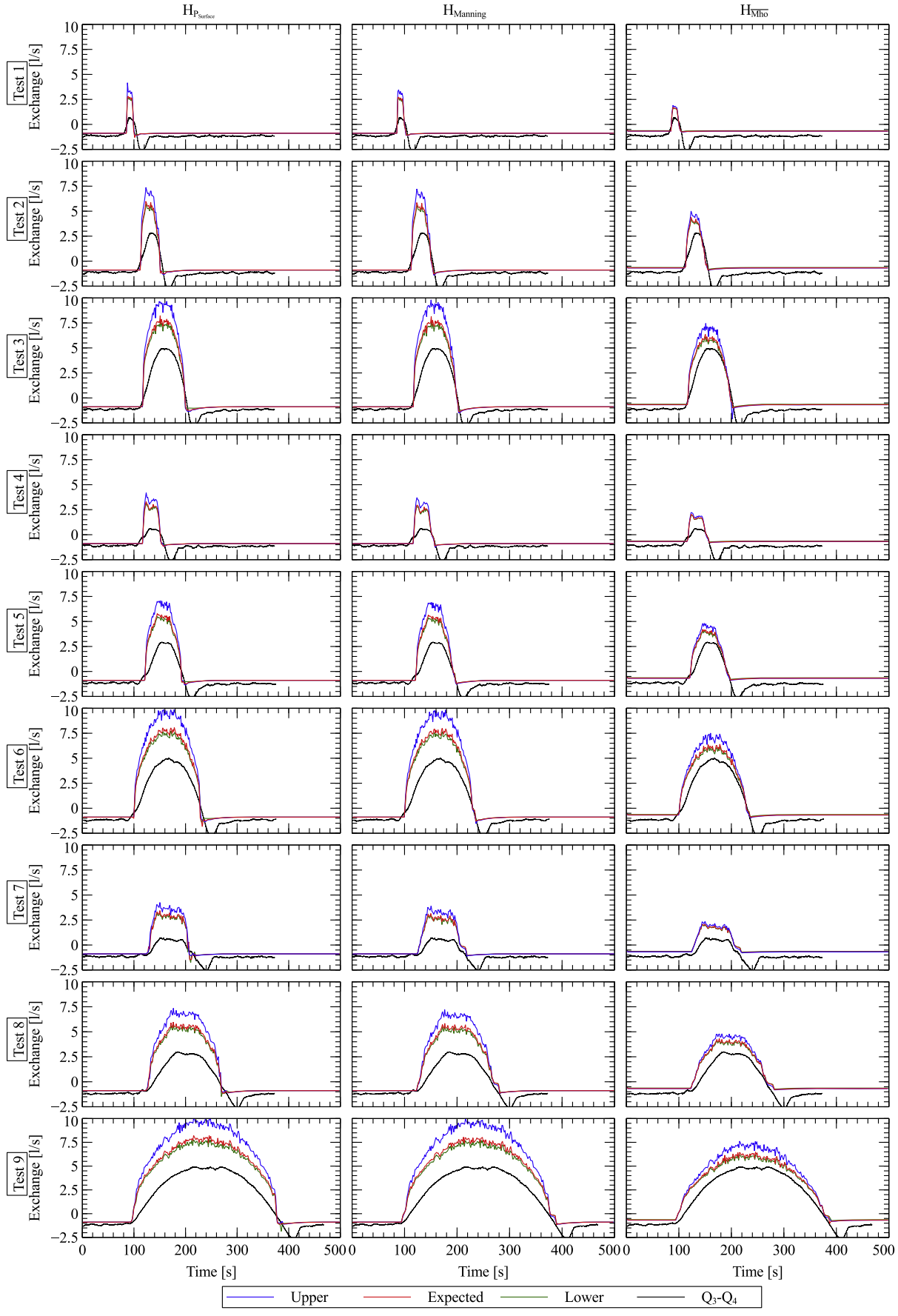

Fig. 10. Experimental flow exchange hydrographs compared with the numerical ones using different parameters discussed in Section 3.2.1.

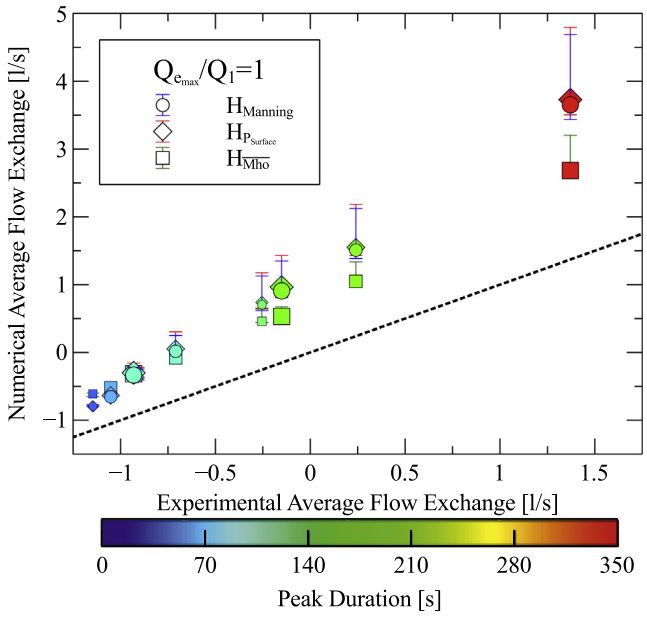

Fig. 11. Comparison between Experimental and Numerical Average Flow Exchange for all the unsteady tests conducted.

lower head differential in surcharged conditions (resulting in lower exchange rates, as discussed above). However free weir drainage conditions are better represented by $H_{P_{Surface}}$. Overall $H_{Manning}$ and $H_{P_{Surface}}$ present very similar results as the influence from the orifice is limited at the $H_{P_{Surface}}$ point and the flow almost exclusively influenced by upstream conditions. The modelling results are relatively sensitive to both the computing point selected on the floodplain system and the discharge coefficient. All numerical models fail to replicate the rapid fluctuation observed to occur at the end of the surcharging flow period (e.g. for event 8 between 280 and 320 s). This transient phenomena was observed during the experimental tests and is due to suction effects which occur during the transition between flow states. A 3D CFD model with a more complex turbulence model would be required to fully replicate this effect, however the scale of the effect is likely not to be significant for 2D flood modelling applications.

5. Concluding remarks

The paper presents calibrated values of discharge coefficients for weir and orifice equations to represent sewer-to-surface and surface-to-sewer flow interaction during urban flood events in the case of exchange through a manhole structure with no lid. For the tests conducted, the range of discharge coefficients is identified to be between 0.493 and 0.587 for the weir equation, between 0.054 and 0.057 for the submerged weir equation and between 0.159 and 0.174 for the orifice equation. It has been demonstrated that such equations can replicate exchange appropriately in steady flows with constant coefficient values if the scenarios for implementation are interpreted correctly. Therefore, the proposed coefficients are recommended for use in Eqs. (1)–(4) to reduce uncertainty and improve accuracy of treating sewer-surface interactions in urban flood modelling. However, the results also highlight that linking equations are sensitive to calculations of relative head within pipe and surface systems, hence the uncertainty related to head losses at hydraulic structures, surface roughness and other parameters in urban hydrology may have significant implications for relative head calculations at these interaction nodes.

To explore the performance of steady state calibrated models in unsteady conditions, the experimental data sets have been used to calibrate a finite volume shock-capturing scheme employed to solve the SWE on a non-uniform 2D mesh. The numerical model has been tested against nine unsteady events with a range of surcharge durations and peak flow exchange simulated within the experimental facility. Experimental *vs* numerical results showed that the model overestimated the values of surcharge flow rate. This could be attributed to the more intense turbulence brought by unsteady nature of the flow, which results in substantial additional head losses during net sewer-to-surface exchange that are not accounted for in steady state conditions. To reduce errors in flood modelling applications for unsteady events, future work should focus on the quantification of these additional unsteady head losses and investigate relationships with the nature of the surcharging flow event. Additionally, future work should investigate the effects of different lid and cover designs on the scale and nature of flow exchange, surface to sewer interaction flows during super-critical surface flows and/or very low flow depths as well as behaviour under more complex two phase air/water flows which have not been investigated by the tests conducted here. Overall, the results presented in this paper can be straightforwardly incorporated in any dual drainage model as recommended standard parameters and reasonable ranges of values for discharge coefficients.

Acknowledgements

The research has been supported by the UK Engineering and Physical Sciences Research Council (grants ID: EP/K040405/1).

Appendix A. Supplementary data

Supplementary data associated with this article can be found, in the online version, at http://dx.doi.org/10.1016/j.jhydrol.2017.06.024.

References

Ata, R., Pavan, S., Khelladi, S., Toro, E.F., 2013. A Weighted Average Flux (WAF) scheme applied to shallow water equations for real-life applications. Adv. Water Resour., 155–172 http://dx.doi.org/10.1016/j.advwatres.2009.02.010.

Balmforth, D., Digman, C., Kellagher, R., David, B., 2006. Desiging for exceedance in urban drainage-good practice, Technical Report.

Bautista-Capetillo, C., Robles, O., Junez-Ferreira, H., Playan, E., 2013. Discharge coefficient analysis for triangular sharp-crested weirs using low-speed photographic technique. J. Irrig. Drain. Eng. 140.

Bazin, P., Nakagawa, H., 2014. Modeling flow exchanges between a street and an underground drainage pipe during urban floods. J. Hydraul. Eng. 140, 1–10. http://dx.doi.org/10.1061/(ASCE)HY.1943-7900.0000917.

Borsche, R., Klar, A., 2014. Flooding in urban drainage systems: Coupling hyperbolic conservation laws for sewer systems and surface flow. Int. J. Numer. Meth. Fluids 76, 789–810. http://dx.doi.org/10.1002/fld.3957.

Cea, L., Garrido, M., Puertas, J., 2010. Experimental validation of two-dimensional depth-averaged models for forecasting rainfall–runoff from precipitation data in urban areas. J. Hydrol. 382, 88–102. http://dx.doi.org/10.1016/j.jhydrol.2009.12.020.

Chen, A., Djordjević, S., Leandro, J., Savić, D., 2007. The urban inundation model with bidirectional flow interaction between 2D overland surface and 1D sewer networks, in: NOVATECH 2007. pp. 465–472.

Chen, A., Leandro, J., Djordjević, S., Schumann, A., 2015. Modelling sewer discharge via displacement of manhole covers during flood events using 1D/2D SIPSON/P-DWave dual drainage simulations. Urban Water J. http://dx.doi.org/10.1080/1573062X.2015.1041991.

Djordjević, S., Prodanović, D., Maksimović, C., Ivetić, M., Savić, D., 2005. SIPSON-simulation of interaction between pipe flow and surface overland flow in networks. Water Sci. Technol. 52, 275–283.

Djordjević, S., Saul, A.J., Tabor, G.R., Blanksby, J., Galambos, I., Sabtu, N., Sailor, G., 2013. Experimental and numerical investigation of interactions between above and below ground drainage systems. Water Sci. Technol. 67, 535–542. http://dx.doi.org/10.2166/wst.2012.570.

Fernandez, A., Najafi, M.R., Durand, M., Mark, B.G., Moritz, M., Jung, H.C., Neal, J., Shastry, A., Laborde, S., Phang, S.C., Hamilton, I.M., Xiao, N., 2016. Testing the skill of numerical hydraulic modeling to simulate spatio-temporal flooding

patterns in the logone floodplain, cameroon. J. Hydrol. 539, 265–280. http://dx.doi.org/10.1016/j.jhydrol.2016.05.026.
Fraga, I., Cea, L., Puertas, J., 2015. Validation of a 1D–2D dual drainage model under unsteady part-full and surcharged sewer conditions. Urban Water J. 9006, 1–11. http://dx.doi.org/10.1080/1573062X.2015.1057180.
Hundecha, Y., Sunyer, M.A., Lawrence, D., Madsen, H., Willems, P., Bürger, G., Kriaučiūnienė, J., Loukas, A., Martinkova, M., Osuch, M., Vasiliades, L., von Christierson, B., Vormoor, K., Yücel, I., 2016. Inter-comparison of statistical downscaling methods for projection of extreme flow indices across Europe. J. Hydrol. 541, 1273–1286. http://dx.doi.org/10.1016/j.jhydrol.2016.08.033.
Kesserwani, G., Wang, Y., 2014. Discontinuous galerkin flood model formulation: Luxury or necessity? Water Resour. Res. 50, 6522–6541. http://dx.doi.org/10.1002/2013WR014906.
Leandro, J., Chen, A., Djordjević, S., Savić, D., 2009. Comparison of 1D/1D and 1D/2D coupled (sewer/surface) hydraulic models for urban flood simulation. J. Hydraul. Eng. 135, 495–504. http://dx.doi.org/10.1061/(ASCE)HY.1943-7900.0000037.
Leandro, J., Chen, A., Schumann, A., 2014. A 2D parallel diffusive wave model for floodplain inundation with variable time step (P-DWave). J. Hydrol. 517, 250–259. http://dx.doi.org/10.1016/j.jhydrol.2014.05.020.
Leandro, J., Lopes, P., Carvalho, R., Páscoa, P., Martins, R., Romagnoli, M., 2014. Numerical and experimental characterization of the 2D vertical average-velocity plane at the center-profile and qualitative air entrainment inside a gully for drainage and reverse flow. Comput. Fluids 102, 52–61. http://dx.doi.org/10.1016/j.compfluid.2014.05.032.
Leandro, J., Martins, R., 2016. A methodology for linking 2D overland flow models with the sewer network model SWMM 5.1 based on dynamic link libraries. Water Sci. Technol. 73.
Lee, J., Chan, H., Huang, C., Leu, J., 2012. Experiments on hydraulic relations for flow over a compound sharp-crested weir. Int. J. Phys. Sci. 7. http://dx.doi.org/10.5897/IJPS11.1695.
Lee, S., Nakagawa, H., Kawaiake, K., Zhang, H., 2013. Experimental validation of interaction model at storm drain for development of integrated urban. J. Jpn. Soc. Civil Eng., Ser. B 1 (69), 109–114.
Lee, S., Nakagawa, H., Kawaike, K., Zhang, H., 2015. Urban inundation simulation considering road network and building configurations. J. Flood Risk Manage., 1–10 http://dx.doi.org/10.1111/jfr3.12165.
Liang, Q., Marche, F., 2009. Numerical resolution of well-balanced shallow water equations with complex source terms. Adv. Water Resour., 873–884 http://dx.doi.org/10.1016/j.advwatres.2009.02.010.
Liang, Q., Marche, F., 2009. Numerical resolution of well-balanced shallow water equations with complex source terms. Adv. Water Resour. 32, 873–884. http://dx.doi.org/10.1016/j.advwatres.2009.02.010.
Lopes, P., Leandro, J., Carvalho, R., Páscoa, P., Martins, R., 2015. Numerical and experimental investigation of a gully under surcharge conditions. Urban Water J. 12, 468–476. http://dx.doi.org/10.1080/1573062X.2013.831916.
Maksimović, C., Prodanović, D., Boonya-Aroonnet, S., Leitão, J.A.P., Djordjević, S., Allitt, R., 2009. Overland flow and pathway analysis for modelling of urban pluvial flooding. J. Hydraul. Res. 47, 512–523. http://dx.doi.org/10.1080/00221686.2009.9522027.
Mark, O., Weesakul, S., Apirumanekul, C., Boonya Aroonnet, S., Djordjević, S., 2004. Potential and limitations of 1 d modelling of urban flooding. J. Hydrol. 299, 284–299. http://dx.doi.org/10.1016/j.jhydrol.2004.08.014.
Martins, R., Leandro, J., Carvalho, R., 2014. Characterization of the hydraulic performance of a gully under drainage conditions. Water Sci. Technol. 69, 2423–2430. http://dx.doi.org/10.2166/wst.2014.168.
Martins, R., Leandro, J., Djordjević, S., 2015. A well balanced Roe Scheme for the local inertial equations with an unstructured mesh. Adv. Water Resour. 83, 351–363. http://dx.doi.org/10.1016/j.advwatres.2015.07.007.
Martins, R., Leandro, J., Djordjević, S., 2016. Influence of sewer network models on urban flood damage assessment based on coupled 1D/2D models. J. Flood Risk Manage. http://dx.doi.org/10.1111/jfr3.12244.
Massey, B., 1998. Mechanics of Fluids. seventh ed.
Mignot, E., Paquier, A., Haider, S., 2006. Modeling floods in a dense urban area using 2 d shallow water equations. J. Hydrol. 327, 186–199. http://dx.doi.org/10.1016/j.jhydrol.2005.11.026.
Palla, A., Colli, M., Candela, A., Aronica, G., Lanza, L., 2016. Pluvial flooding in urban areas: the role of surface drainage efficiency. J. Flood Risk Manage. http://dx.doi.org/10.1111/jfr3.12246.
Ravazzani, G., Amengual, A., Ceppi, A., Homar, V., Romero, R., Lombardi, G., Mancini, M., 2016. Potentialities of ensemble strategies for flood forecasting over the milano urban area. J. Hydrol. 539, 237–253. http://dx.doi.org/10.1016/j.jhydrol.2016.05.023.
Reda, M., Abd El-Hady, R., 2011. 2D–3D Modeling of flow over sharp-crested weir. Appl. Sci. Res. 7.
Rubinato, M., 2015. Physical Scale Modelling of Urban Flood Systems. (Ph.D thesis). The University of Sheffield, 2015. URL http://etheses.whiterose.ac.uk/id/eprint/9270.
Rubinato, M., Shucksmith, J., Saul, A., Shepherd, W., 2013. Comparison between InfoWorks hydraulic results and a physical model of an urban drainage system. Water Sci. Technol., 372–379 http://dx.doi.org/10.2166/wst.2013.254.
Russo, B., Gómez, M., Tellez, J., 2013. Methodology to estimate the hydraulic efficiency of nontested continuous transverse grates. J. Irrig. Drain. Eng. 139, 864–871. http://dx.doi.org/10.1061/(ASCE)IR.1943-4774.0000625.
Schmitt, T.G., Thomas, M., Ettrich, N., 2004. Analysis and modeling of flooding in urban drainage systems. J. Hydrol. 299, 300–311. http://dx.doi.org/10.1016/j.jhydrol.2004.08.012.
Schöberl, J., 1997. NETGEN An advancing front 2D/3D-mesh generator based on abstract rules. Comput. Visualization Sci. 1, 41–52. http://dx.doi.org/10.1007/s007910050004.
Seyoum, S., Vojinovic, Z., Price, R., Weesakul, S., 2012. Coupled 1D and noninertia 2D flood inundation model for simulation of urban flooding. J. Hydraul. Eng. 138, 23–34. http://dx.doi.org/10.1061/(ASCE)HY.1943-7900.
Smith, M.B., 2006. Comment on analysis and modeling of flooding in urban drainage systems. J. Hydrol. 317, 355–363. http://dx.doi.org/10.1016/j.jhydrol.2005.05.027.
Song, L., Zhou, J., Guo, J., Zou, Q., Liu, Y., 2011. A robust well-balanced finite volume model for shallow water flows with wetting and drying over irregular terrain. Adv. Water Resour., 915–932 http://dx.doi.org/10.1016/j.advwatres.2011.04.017.